RESEARCH ARTICLE

A Tandem-Locked Chemiluminescent Probe for Imaging of Tumor-Associated Macrophage Polarization

Jingsheng Huang,[a] Mengke Xu,[a] Penghui Cheng,[a] Jie Yu,[a] Jiayan Wu,[a] Kanyi Pu*[a],[b]

[a] Dr. J. Huang, M. Xu, Dr. P. Cheng, Dr. J. Yu, Dr. J. Wu, and Prof. K. Pu
School of Chemistry, Chemical Engineering and Biotechnology, Nanyang Technological University, Singapore 637457, Singapore
[b] Prof. K. Pu
Lee Kong Chian School of Medicine, Singapore 636921, Singapore
E-mail: kypu@ntu.edu.sg

Supporting information for this article is given via a link at the end of the document.

Abstract: Tumor-associated macrophages (TAMs) play a role in both pro-and anti-tumor functions; and the targeted polarization from M2 to M1 TAMs has become an effective therapy option. Although detection of M1 TAMs is imperative to assess cancer immunotherapeutic efficacy, existing optical probes suffer from shallow tissue penetration depth and poor specificity toward M1 TAMs. Herein, we report a tandem-locked NIR chemiluminescent (CL) probe for specific detection of M1 TAM. Through a combined molecular engineering approach via both atomic alternation and introduction of electron-withdrawing groups, near-infrared (NIR) chemiluminophores are screened out to possess record-long emission (over 800 nm), record-high CL quantum yield (2.7% einstein/mol), and prolonged half-life (7.7 h). Based on an ideal chemiluminophore, the tandem-locked probe (DPD_{GN}) is developed to only activate CL signal in the presence of both tumour (γ-glutamyl transpeptidase) and M1 macrophage biomarkers (nitric oxide). Such a tandem-lock design ensures its high specificity towards M1 macrophages in the tumor microenvironment over those in normal tissues or peripheral blood. Thus, DPD_{GN} permits noninvasive imaging and tracking of M1 TAM activation in the tumor of living mice during R837 treatment, showing a good correlation with ex vivo methods. This study not only reports a new molecular approach towards highly efficient chemiluminophores but also reveals the first tandem-locked CL probes for enhanced imaging specificity.

Introduction

Cancer immunotherapy, which stimulates the patients' own immune system to fight cancer, provides long-lasting protection against cancer.[1-2] The infiltration and activation of leukocytes in the tumor microenvironment (TME) are closely associated with cancer progression and patient responses to immunotherapy.[3] In particular, tumor-associated macrophages (TAMs) represent one of the main tumor-infiltrating immune cell types and play both anti- and pro-tumor functions based on different phenotypes.[4-5] In contrast to M2 TAMs that promote tumor cell proliferation and invasion, M1 TAMs have anti-tumor effects and trigger tumor cell death by either directly releasing cytotoxic reactive oxygen species and nitric oxide (NO), or antibody-dependent cell-mediated cytotoxicity.[5] Therefore, targeted M1 TAM polarization from naive M0 macrophages and repolarization of M2 to M1 TAMs are effective tumor treatment options. To enable prognosis and improved patient outcomes, detection of M1 TAM activation during immunotherapy is essential. However, current clinical diagnostic approaches include histological,[6] flow cytometry,[6-7] or mass cytometry analyses of tumor specimens from biopsy,[7] are invasive and suffer from risks of excessive bleeding and tumor cell seeding.[8]

Molecular imaging that sensitively detects biomarkers of interest offers a noninvasive approach to visualize biological processes at the cellular or subcellular levels in both fundamental studies and clinical practice.[9-13] To detect M1 macrophage activation and repolarization, fluorescence imaging agents have been reported to actively target biomarkers such as GLUT1 glucose transporter, and SLC18B1 transporter, which however show “always on” signal and thus background signal from nonspecific accumulation of probes.[14-15] Moreover, activatable fluorescent probes that specifically turn on their fluorescence in the presence of biomarkers of M1 macrophages (such as NO, low pH and hypochlorite) have been developed.[16-20] However, the activatable fluorescent probes fail to distinguish M1 TAMs over that in normal tissues or peripheral blood. Besides, they share the general drawback of fluorescence imaging that is tissue autofluorescence, resulting in poor signal-to-background ratio (SBR).[21-22]

Without the requirement of real-time light excitation, chemiluminescence (CL) imaging have minimized background noise and thus higher SBR than fluorescence imaging.[23-27] Recently, biomarker-activatable CL probes have been reported for detection of a variety of biomarkers, including enzymes,[28-35] reactive oxygen and nitrogen species,[10], [36-43] and metabolites.[44-45] However, these CL probes typically emit visible light, and only nine of them emit near-infrared region (NIR) light. Besides, these CL probes suffer from drawbacks such as poor CL quantum yields and short CL half-lives, which significantly hinder *in vivo* imaging applications. Despite the potential of CL imaging in in vivo detection of macrophage polarization, the challenges lie in the synthesis of highly efficient NIR CL probes with high specificity towards macrophages in the tumor tissue over normal tissues.

In this study, we report a hydrophilic tandem-locked biomarker-activatable CL probe (DPD_{GN}) for in vivo detection of tumor-associated macrophage repolarization. To ensure high specificity toward macrophages in TME, NO and gamma-glutamyl transferase (GGT) were chosen as the biomarkers for macrophages and cancer cells, respectively.[46-47] Such a tandem strategy for designing activatable fluorescent probes is widely used.[48] In this way. the CL signal of DPD_{GN} is only turned-on by

M1 TAM. To screen out highly efficient NIR chemiluminophores, a combined molecular engineering approach involving both atomic alternation and introduction of electron-withdrawing group (EWG) was introduced into the adamantyliene-1,2-dioxetane scaffolds. Such a combined molecular engineering approach results in red-shifted emission wavelength (750 - 820 nm), prolonged CL half-lives ($t_{1/2Cl}$ = 0.8 - 7.7 h), and a high CL quantum yield (Φ_{Cl} = 0.1 - 2.7% einstein/mol). Note that both CL half-lives and emission of 7.7 h and 820 nm are record-longer than existing chemiluminophores (**Table S1**). The best performer (DPD_O, λ_{em} = 750 nm, Φ_{Cl} = 2.7%, $t_{1/2Cl}$ = 7.7 h) was subsequently developed into the tandem-locked CL probe (DPD_{GN}) for real-time imaging of M1 TAM activation in the tumor mouse model.

Results and Discussion

The NIR chemiluminophores (DPD_O, DPD_S, BPD_O, and BPD_S) were synthesized via a convergent approach based on Schaap's dioxetane scaffold (**Scheme S1**). Briefly, 2-methyl-4H-chromen-4-one (compound 1o) and 2-methyl-4H-thiochromen-4-one (compound 1s) respectively reacted with 1,3-indanedione and benzo[b]thiophen-3(2H)one-1,1-dioxide to yield the corresponding acceptors (compound 2o or 2s) via Knoevenagel condensation. The chemiluminophore precursors were then obtained by Knoevenagel reaction between the respective acceptors and hydroxybenzaldehyde-adamantan-2-ylidene (HBAY); and subsequently, the chemiluminophores were synthesized by photosensitized oxidation of their precursors. The structures of all chemiluminophores were confirmed by ^{1}H, ^{13}C nuclear magnetic resonance (NMR), and liquid chromatography-mass spectrometry (LC-MS) analyses (supporting information).

The photophysical properties of four chemiluminophores were studied by measuring their UV/vis absorption, fluorescence, and CL spectra. As shown in **Figure 1a-b**, all four chemiluminophores showed similar absorption spectra with maxima around 500 nm. The CL emission of DPD_O, DPD_S, BPD_O, and BPD_S had the maxima at ~ 750, 800, 760 and 820 nm, respectively (**Figure 1c**). In particular, sulfur-substituted DPD_S and BPD_S had the record-long CL emission (≥ 800 nm) among reported chemiluminophores (**Table S1** and **Figure 1e**).[30], [33], [35] This red-shifted emission could be attributed to the increased atomic radius and change in electronegativity.[49] Besides, the chemiluminophores that contained strong EWGs (sulfuryl group) exhibited slightly red-shifted CL emission (DPD_S: 760 nm; BPD_S: 820 nm) than their corresponding ketone-substituted chemiluminophores (DPD_O: 750 nm; BPD_O: 800 nm). The CL spectra of all four chemiluminophores coincided well with their fluorescence spectra of activated forms (**Figure S1b**). All chemiluminophores exhibited long CL half-lives due to intermolecular H-bonding: DPD_O (~7.7 h), DPD_S (5.7 h), BPD_O (3.2 h), and BPD_S (0.8 h). In addition, the CL quantum yield (Φ_{Cl}) of DPD_O (2.7%) was the highest among all chemiluminophores (DPD_S/1.0%, BPD_O/0.6%, and BPD_S/0.1%), and also much higher than most of literature reported NIR chemiluminophores (**Table S1** and **Figure 1e**). The low Φ_{Cl} of BPD_O and BPD_S was ascribed to low fluorescence quantum yield of activated forms due to twisted intramolecular charge transfer (TICT) effect. Thus, combined molecular engineering approach endows NIR chemiluminophores with redshift CL emission and high Φ_{Cl}. After considering the physical properties, DPD_O with the outstanding CL quantum yield and desired long half-life was selected for subsequent *in vivo* imaging.

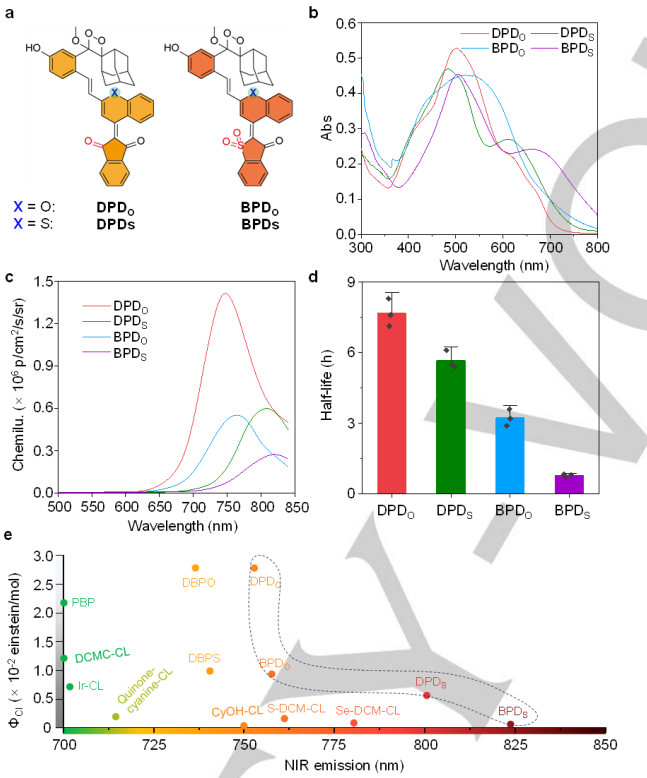

Figure 1. **(a)** Molecular design of NIR chemiluminophores based on Schaap's dioxetane scaffold with different substituent groups. UV/Vis absorption spectra **(b)**, CL spectra **(c)**, and half-lives **(d)** of DPD_O, DPD_S, BPD_O, and BPD_S (50 μM) in PBS (10 mM, pH 7.4, 40% DMSO), respectively (n = 3 independent experiments, mean ± s.d.). (**e**) CL quantum yields and maximum CL emissions of reported NIR chemiluminophores and our design highlighted with circle.

To achieve specific detection of tumor-associated macrophage polarization, a hydrophilic dual-locked NIR CL probe (DPD_{GN}) was developed (**Figure 2a**). DPD_{GN} was designed by caging the hydroxyl group of DPD_O with a self-immolative linker (*p*-aminobenzyl alcohol) connected to a GGT-cleavable γ-glutamate, and the carboxyl group of γ-glutamate was further locked by a NO-cleavable o-phenylenediamine. To improve its water solubility for subsequent in vivo applications, an azide group was introduced onto modified chemiluminophore (compound 17), which was then conjugated with DBCO-mPEG2k to afford DPD_{GN}. As shown in **Figure 2b** and **Scheme S2**, the brominated tandem-locked responsive group with alloc protection was conjugated to the green chemiluminophore precursor HYCL to afford compound 15, which was then coupled to azide-functionalized compound 8 via Knoevenagel condensation reaction to yield compound 16. Followed by alloc group deprotection and photooxidation, water-soluble moiety PEG2k was introduced onto the dioxetane intermediate compound 17 via copper-free click reaction to afford probe DPD_{GN}. The structures of all compounds were confirmed by ^{1}H, ^{13}C NMR, and LC-MS analyses (supporting information).

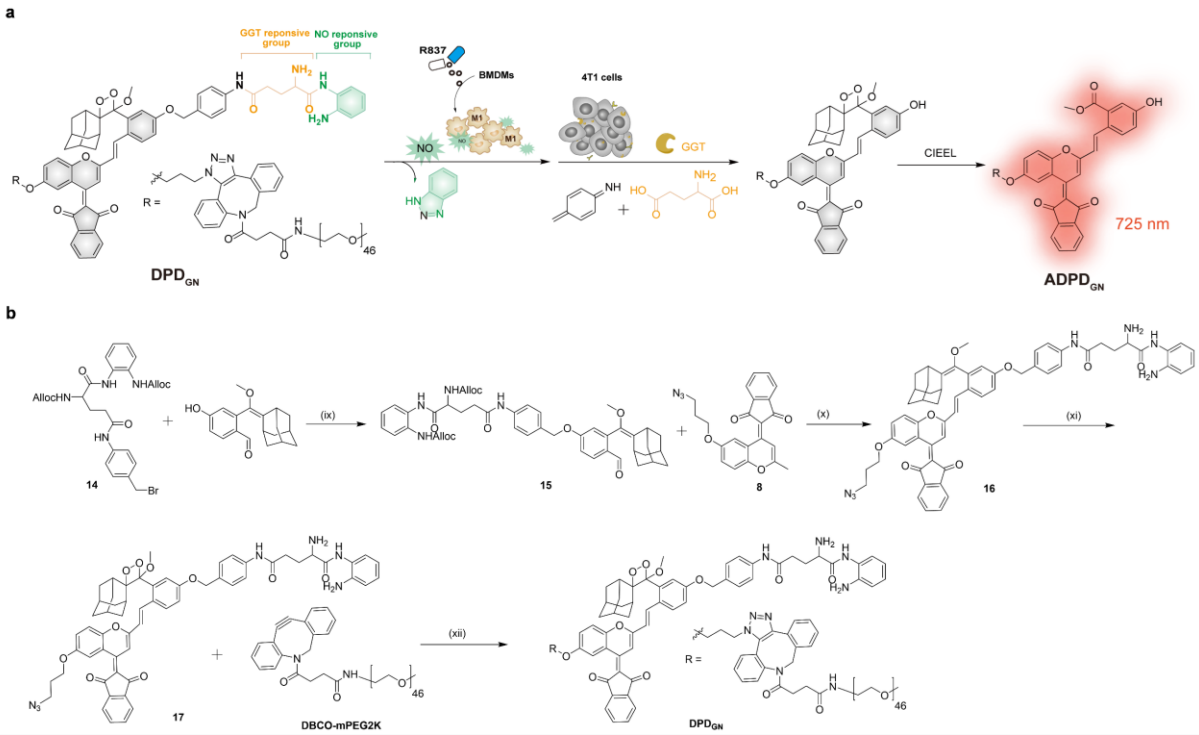

Figure 2. Design and synthesis of hydrophilic tandem-locked NIR chemiluminescent probe DPD$_{GN}$. **(a)** Schematic illustration of the sequential CL signal activation from tandem-locked DPD$_{GN}$ in the presence of both NO from M1 macrophages and GGT from tumor cells. **(b)** Synthetic route of DPD$_{GN}$. Reagents and conditions: (ix) compound 14, HBAY, K_2CO_3, Cs_2CO_3, acetonitrile, N_2, 4 h, room temperature (r.t.), 62% yield; (x) compounds 15 and 8, piperidine, Acetonitrile, reflux, 2 h; $Pd(Pph_3)_4$, 1,3-dimethylbarbituric acid, tetrahydrofuran, r.t., 4 h, 37% product yield; (xi) compound 17, methylene blue, white light, air, 0 °C, 2 h, 92% product yield; (xii) DBCO-mPEG2k, dichloromethane, 0 °C, 2 h, ~100% product yield.

The sensing capability of DPD$_{GN}$ was tested by measuring CL spectra in the presence or absence of the biomarkers-of-interest. As shown in **Figure 3a**, DPD$_{GN}$ intrinsically exhibited minimal CL signals, but showed a 26.6-fold CL enhancement at 725 nm in the presence of both biomarkers (NO and GGT). In comparison, its fluorescence only increased by ~ 1.7-fold in the presence of both biomarkers because of the low fluorescence increase after cleavage (**Figure 3b, S2b**). This should be caused by the limited changes in intramolecular charge transfer process that methyl benzoate of activated form (ADPD$_O$) could reduce the donation ability of oxygen of phenol. Meanwhile, the absorption maximum shifted from 476 to 465 nm, which was the characteristic peak of ADPD$_O$ (**Figures S2a**&**S1a**). In contrast, no CL or fluorescence enhancement was observed for DPD$_{GN}$ when only one biomarker or other interfering enzymes was present (**Figure 3c**). The specificity was further confirmed by minimal CL enhancement after adding GGsTop (a potent GGT inhibitor) into the mixture of DPD$_{GN}$, NO, and GGT. Moreover, the CL signal of DPD$_{GN}$ drastically enhanced and reached plateau within 20 min, followed by a slow decay with a half-life of 198 min (**Figure S2c**). As validated by HPLC and LCMS analyses (**Figure S3a**), a new HPLC peak appeared at 15.2 min corresponding to activated compound 17 (molecular weight: 549.2) (**Figure S3b**), proving the sequential biomarker activation mechanism of DPD$_{GN}$ precursor (compound 17) by NO and GGT. Moreover, the limit of detection (LOD) for DPD$_{GN}$ to detect GGT was determined to be 0.12 U/L, which was more sensitive than other existing probes (**Figure S2d**).

The sensing capability of DPD$_{GN}$ towards macrophage polarization was then tested in living cells after confirming its low cytotoxicity (**Figure S4**). To stimulate macrophage polarization in the TME, murine bone marrow-derived macrophages (BMDMs) and mammary carcinoma cells (4T1) were seeded in the lower and upper compartments of a transwell plate, respectively (**Figure 3d**). The BMDMs in the lower compartment were firstly treated with imiquimod (R837, an immune response modifier and a selective toll like receptor 7 agonist) for 0 (R837^{0h}), 36 (R837^{36h}) or 72 h (R837^{72h});[50] before the 4T1-seeded upper compartment was introduced. The cell co-culture was then incubated with DPD$_{GN}$ (30 μM, 20 min) before CL imaging. As shown in **Figure 3e**, CL signals from cell culture in R837^{72h} group was 1.7, 4.3-fold higher than R837^{36h} and R837^{0h}, respectively. No obvious CL signals from DPD$_{GN}$ solely incubated with BMDM or 4T1 cells was observed, demonstrating tandem-locked DPD$_{GN}$ showed a specific activation in the cell level. Flow cytometry analyses was conducted, showing the percentages of M1 macrophages (iNOS$^+$CD206$^-$) from R837^{72h} group was ~2.0, 4.3-fold higher than R837^{36h} and R837^{0h} groups, respectively (**Figure 3f**). Moreover, population of M2 macrophages was continually decreased after prolonging R837 treatment. This trend was similar to the CL signals as it showed a very high correlation between CL intensity and population of M1 macrophage, confirming that the CL signals from activated DPD$_{GN}$ were specific to M1 macrophages (**Figure 3g**). Thus, DPD$_{GN}$ specifically detected the polarization of macrophage to M1 macrophages.

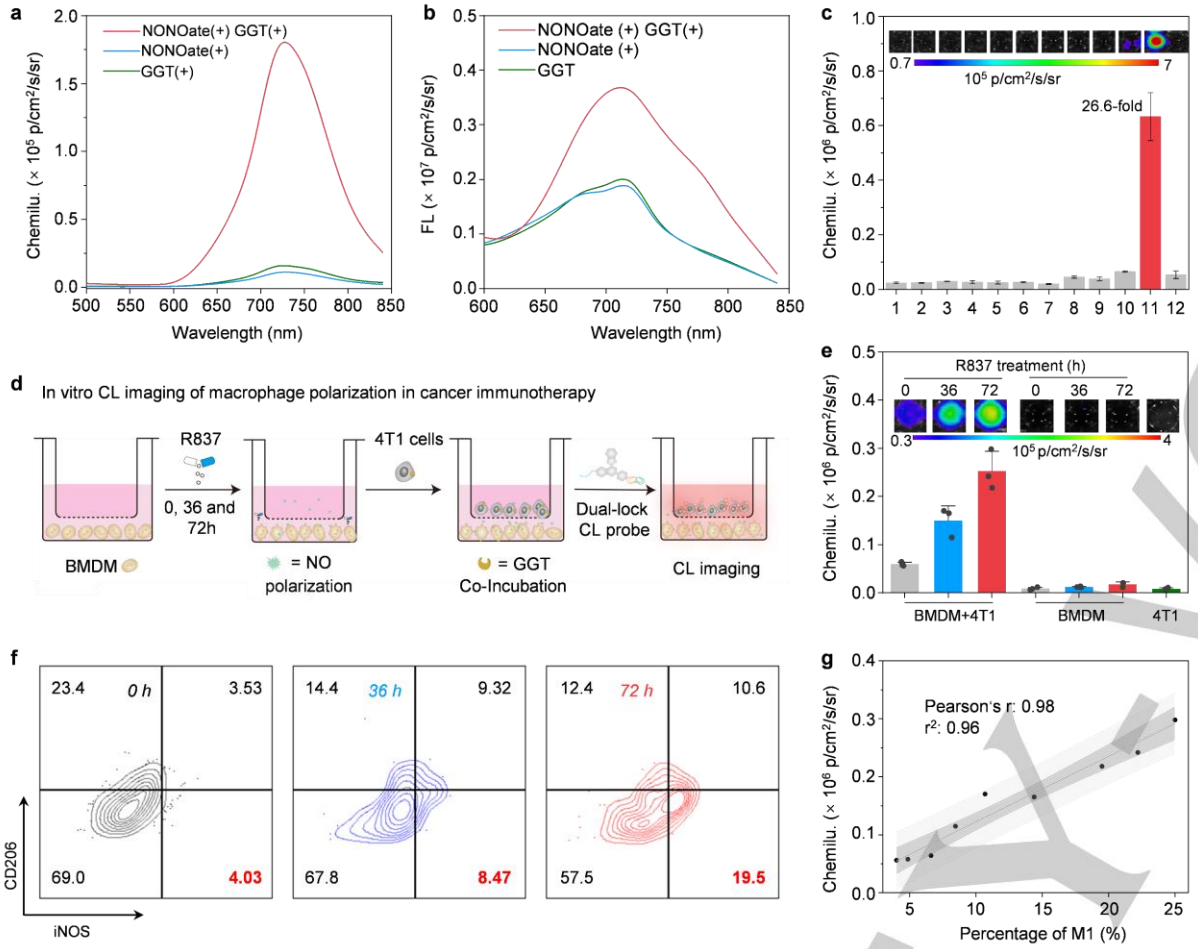

Figure 3. In vitro characterization of the detection capabilities of DPD_{GN}. CL spectra **(a)** and fluorescence spectra (**b**) of DPD_{GN} (30 μM) in the presence of individual biomarkers or combined biomarkers in PBS (10 mM, pH 7.4) at 37 °C. For the individual biomarker, NONOate (NO donor, 60 μM) or GGT enzyme (~10 U/L) was added to a solution of DPD_{GN} for 30 min incubation. For combined biomarkers, GGT was added and incubated for another 30 min following NONOate incubation for 30 min. **(c)** CL signal changes of DPD_{GN} (30 μM) after incubation with different enzymes (ALP, CatB, DPP_{IV}, furin, β-gal, NTR, uPA, GGT, or NONOate for 30 min incubation at 37 °C in PBS buffer. Different groups on X axis: 1: PBS, 2: ALP, 3: CatB, 4: DPP_{IV}, 5: furin, 6: β-gal, 7: NTR, 8: uPA, 9: GGT, 10: NONOate, 11: NONOate + GGT, 12: NONOate + GGT + GGsTop. Group NONOate + GGT + GGsTop: GGT inhibitor (GGsTop, 0.2 mM) was treated 6 h earlier than the combined biomarker incubation. **(d)** Schematic illustration for CL imaging of tumor-associated macrophage polarization. BMDM means bone marrow-derived macrophages. **(e)** CL intensity of BMDM+4T1 group and BMDM group treated with R837 (10 μg mL^{-1}) at different treatment times (0, 36 and 72 h), and 4T1 group without R837 treatment. **(f)** Flow cytometry analysis of M1 ($iNOS^+CD206^-$) and M2 macrophages ($iNOS^-CD206^+$) polarization from BMDMs at post-treatment with R837 (10 μg mL^{-1}). **(g)** Correlation studies between percentages of tumor-infiltrating M1-type macrophages ($iNOS^+CD206^-$) and CL intensity of turn-on DPD_{GN}.

The ability of DPD_{GN} for real-time imaging of tumor-associated macrophage polarization was tested in lung metastasis model (**Figure 4a**). BALB/c mice received intravenous injection of 4T1 cells and received R837 (a TLR7 agonist) 14 days post-tumor implantation. Tumor-bearing mice received R837 (1.25 mg Kg^{-1}) for three dosages with an interval of 48 h.[51] For the control group, tumor-bearing mice were pre-treated with GGsTop or treated with PBS. At day 20, DPD_{GN} was intratracheally injected into living mice, and longitudinal CL imaging were conducted for 4 h post-injection (**Figure 4b**). The CL signal at lung metastatic region was quantitatively studied, a gradual CL signal increase was observed with a signal maximum at 30 min post injection, followed by gradual signal decrease due to body clearance (**Figure 4c**). At 30 min post injection, the CL signal from mice receiving R837 treatment was 4.0, 15.7-fold higher than PBS or GGsTop-treated groups. In contrast, the fluorescence signals from DPD_{GN} activation in mice receiving R837 treatment showed no statistically significant enhancement as compared to the control group (**Figure S5**), which was similar to the in vitro data. To examine the close association of CL signals from activated DPD_{GN} with macrophage polarization, flow cytometry studies were conducted on the lung tissues from different treatment groups (**Figure 4d**). In mice receiving R837-treatment, increased tumor infiltration of tumor infiltration of $iNOS^+CD206^-$ M1 macrophages was 2.1-fold higher than that for PBS-treated groups and decreased M2 TAMs was ~1.7-fold lower than PBS-treated group due to R837-induced polarization from M2 to M1. (**Figure S6**). Histological studies showed significantly suppressed tumor size in R837-treated group as compared to PBS-treated group, demonstrating the anti-tumor effects of M1 macrophages (**Figure 4e**). Moreover, no discernible indications of toxicity within major organs (heart, liver, spleen, and kidneys) were observed, validating the good biosafety of DPD_{GN} (**Figure S7**).

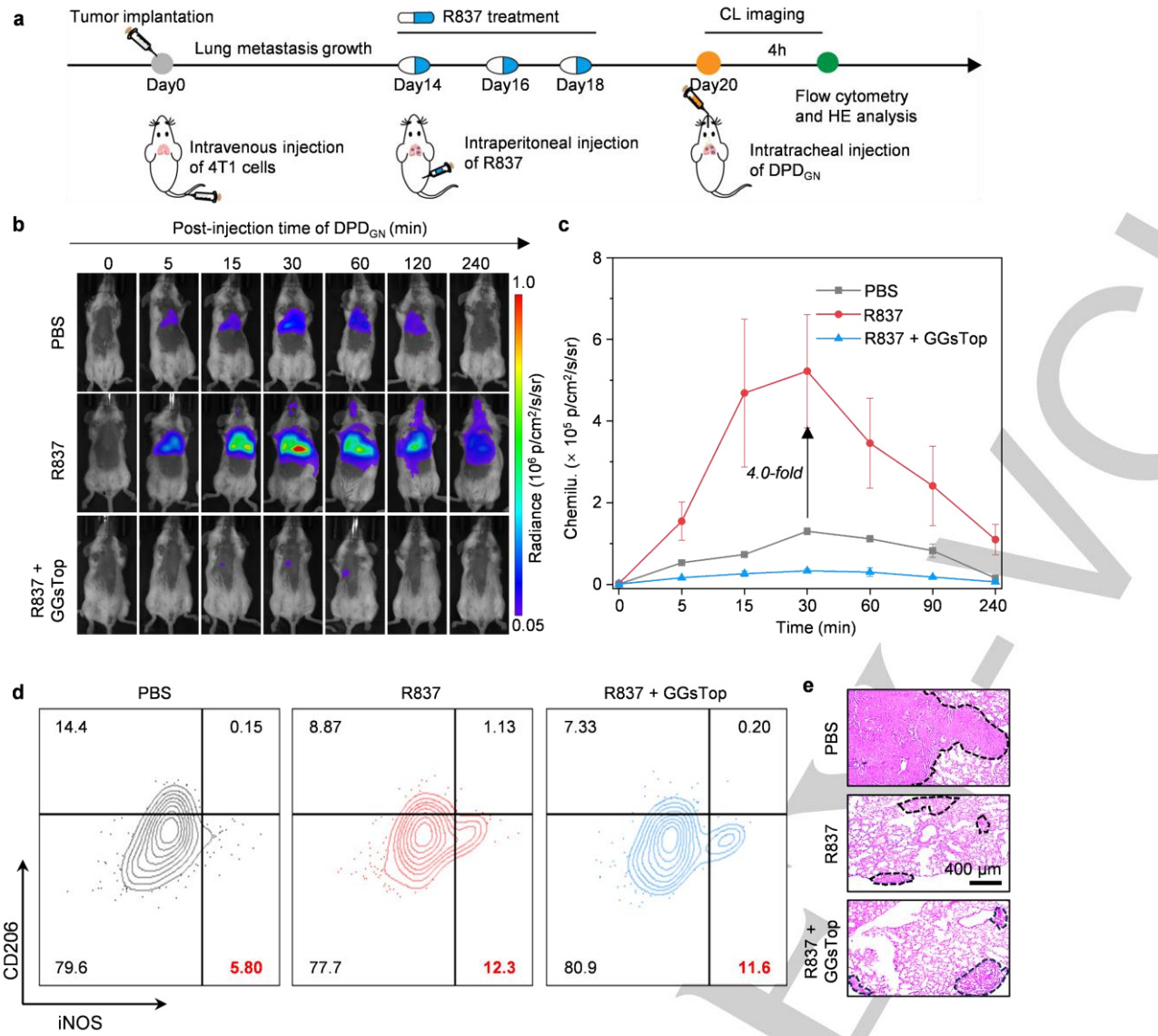

Figure 4. In vivo real-time CL imaging of tumor-associated M1 macrophage. **(a)** Schematic illustration for the timeline of R837 treatment and real-time imaging of DPD_{GN}. 4T1 cells were intravenously injected to living mice at day 0 and then R837 was treated at day 14, 16 and 18 through intraperitoneal injection. DPD_{GN} (2 mM, 10 μL per mouse) was intratumorally administered to living mice at day 20. IF represents immunofluorescence. **(b)** Real-time CL imaging in orthotopic lung tumor after Intratracheal injection of DPD_{GN}. The inhibitor (GGsTop) (20 mg kg^{-1}) was intraperitoneally injected 12 h before CL imaging. **(c)** Quantification of CL signal from the lung area of 4T1-bearing mice in **(b)** (n = 3 independent mice, mean ± s.d.). **(d)** Flow cytometry analysis of M1 ($iNOS^+CD206^-$) and M2 macrophages ($iNOS^-CD206^+$) polarization in lung tumor tissues from each group. **(e)** H&E analysis of lung tissues in each group.

Conclusion

In conclusion, we developed four NIR chemiluminophores (DPD_O, DPD_S, BPD_O, and BPD_S) by a combined molecular engineering approach into the adamantyliene-1,2-dioxetane scaffold. To realize specific detection of M1 TAMs during R837 treatment, well-performed DPD_O with the highest CL quantum yield (2.7% einstein/mol) and the longest CL half-life (~ 7.7 h) was screened out to be constructed into a tandem-locked NIR CL probe (DPD_{GN}). DPD_{GN} is turned-on with 26.6-fold CL emission at 725 nm only in the presence of both NO and GGT, which are biomarkers associated with M1 macrophage and 4T1 cancer cells, respectively. The detection capability of DPD_{GN} was then tested in both living cells and tumor-bearing mice, and the CL signals from activated DPD_{GN} highly correlated to population of TAM activation towards M1-phenotype, which was validated by flow cytometry analyses. Therefore, our study not only provides a combined alternation approach (EWG and atomic alteration) to develop NIR chemiluminophores, but also reports the first tandem-locked CL probes with a bright emission for specific detection of M1 TAM activation.

Acknowledgements

K.P. thanks Singapore National Research Foundation (NRF) (NRF-NRFI07-2021-0005), and Singapore Ministry of Education, Academic Research Fund Tier 1 (2019-T1-002-045, RG125/19,

RT05/20), Academic Research Fund Tier 2 (MOE-T2EP30220-0010; MOE-T2EP30221-0004), for the financial support.

Keywords: chemiluminescent probe • macrophage detection • tandem-lock

Reference

[1] I. Mellman, G. Coukos, G. Dranoff, *Nature* **2011**, *480*, 480-489.
[2] D. G. DeNardo, B. Ruffell, *Nat. Rev. Immunol.* **2019**, *19*, 369-382.
[3] W. H. Fridman, L. Zitvogel, C. Sautès–Fridman, G. Kroemer, *Nat. Rev. Cancer* **2020**, *20*, 662-680.
[4] W. H. Fridman, L. Zitvogel, C. Sautès–Fridman, G. Kroemer, *Nat. Rev. Clin. Oncol.* **2017**, *14*, 717-734.
[5] T. Satoh, O. Takeuchi, A. Vandenbon, K. Yasuda, Y. Tanaka, Y. Kumagai, T. Miyake, K. Matsushita, T. Okazaki, T. Saitoh, K. Honma, T. Matsuyama, K. Yui, T. Tsujimura, D. M. Standley, K. Nakanishi, K. Nakai, S. Akira, *Nat. Immunol.* **2010**, *11*, 936-944.
[6] D. W. Gutkin, M. R. Shurin, *Cancer Immunol. Immunother.* **2014**, *63*, 45-57.
[7] R. Gadalla, B. Noamani, B. L. MacLeod, R. J. Dickson, M. Guo, W. Xu, S. Lukhele, H. J. Elsaesser, A. R. A. Razak, N. Hirano, T. L. McGaha, B. Wang, M. Butler, C. J. Guidos, P. S. Ohashi, L. L. Siu, D. G. Brooks, *Front. Oncol.* **2019**, *9*, 415.
[8] K. Shyamala, H. C. Girish, S. Murgod, *J. Int. Soc. Prev. Community Dent.* **2014**, *4*, 5-11.
[9] S. H. Yun, S. J. J. Kwok, *Nat. Biomed. Eng.* **2017**, *1*, 0008.
[10] J. Huang, J. Li, Y. Lyu, Q. Miao, K. Pu, *Nat. Mater.* **2019**, *18*, 1133-1143.
[11] Y. Chen, S. Wang, F. Zhang, *Nat. Rev. Bioeng.* **2023**, *1*, 60-78.
[12] S. He, P. Cheng, K. Pu, *Nat. Biomed. Eng.* **2023**, *7*, 281-297.
[13] X. Wu, R. Wang, N. Kwon, H. Ma, J. Yoon, *Chem. Soc. Rev.* **2022**, *51*, 450-463.
[14] H. Cho, H.-Y. Kwon, A. Sharma, S. H. Lee, X. Liu, N. Miyamoto, J.-J. Kim, S.-H. Im, N.-Y. Kang, Y.-T. Chang, *Nat. Commun.* **2022**, *13*, 5974.
[15] S.-J. Park, B. Kim, S. Choi, S. Balasubramaniam, S.-C. Lee, J. Y. Lee, H. S. Kim, J.-Y. Kim, J.-J. Kim, Y.-A. Lee, N.-Y. Kang, J.-S. Kim, Y.-T. Chang, *Nat. Commun.* **2019**, *10*, 1111.
[16] Y. Huo, J. Miao, J. Fang, H. Shi, J. Wang, W. Guo, *Chem. Sci*. **2019**, *10*, 145-152.
[17] P. Yuan, X. Xu, D. Hu, Y. Chen, J. Fan, S. Yao, Y. Piao, Z. Zhou, S. Shao, N. K. H. Slater, Y. Shen, J. Tang, *J. Am. Chem. Soc.* **2023**, *145*, 7941-7951.
[18] M. Y. Lucero, A. K. East, C. J. Reinhardt, A. C. Sedgwick, S. Su, M. C. Lee, J. Chan, *J. Am. Chem. Soc.* **2021**, *143*, 7196-7202.
[19] A. Fernandez, M. Vermeren, D. Humphries, R. Subiros-Funosas, N. Barth, L. Campana, A. MacKinnon, Y. Feng, M. Vendrell, *ACS Cent. Sci.* **2017**, *3*, 995-1005.
[20] M. Baruah, H.-Y. Kwon, H. Cho, Y.-T. Chang, A. Samanta, *Anal. Chem.* **2023**, *95*, 4147-4154.
[21] Q. Miao, K. Pu, *Adv. Mater.* **2018**, *30*, 1801778.
[22] J. Li, K. Pu, *Chem. Soc. Rev.* **2019**, *48*, 38-71.
[23] R. Blau, O. Shelef, D. Shabat, R. Satchi-Fainaro, *Nat. Rev. Bioeng.* **2023**, *1*, 648-664.
[24] J. Huang, K. Pu, *Angew. Chem. Int. Ed.* **2020**, *59*, 11717-11731.
[25] Y. Jiang, K. Pu, *Chem. Rev.* **2021**, *121*, 13086-13131.
[26] N. Hananya, D. Shabat, *Angew. Chem. Int. Ed.* **2017**, *56*, 16454-16463.
[27] O. Green, T. Eilon, N. Hananya, S. Gutkin, C. R. Bauer, D. Shabat, *ACS Cent. Sci.* **2017**, *3*, 349-358.
[28] X. Shi, Y. Deng, X. Liu, G. Gao, R. Wang, G. Liang, *Biosens. Bioelectron.* **2022**, *208*, 114212.
[29] Y. Liu, J. Zeng, Q. Li, M. Miao, Z. Song, M. Zhao, Q. Miao, M. Gao, *Adv. Opt. Mater.* **2022**, *10*, 2102709.
[30] O. Green, S. Gnaim, R. Blau, A. Eldar-Boock, R. Satchi-Fainaro, D. Shabat, *J. Am. Chem. Soc.* **2017**, *139*, 13243-13248.
[31] R. An, S. Wei, Z. Huang, F. Liu, D. Ye, *Anal. Chem.* **2019**, *91*, 13639-13646.
[32] J. Cao, J. Campbell, L. Liu, R. P. Mason, A. R. Lippert, *Anal. Chem.* **2016**, *88*, 4995-5002.
[33] J. Huang, C. Zhang, X. Wang, X. Wei, K. Pu, *Angew. Chem. Int. Ed.* **2023**, *62*, e202303982.
[34] J. Huang, P. Cheng, C. Xu, S. S. Liew, S. He, Y. Zhang, K. Pu, *Angew. Chem. Int. Ed.* **2022**, *61*, e202203235.
[35] J. Huang, Y. Jiang, J. Li, J. Huang, K. Pu, *Angew. Chem. Int. Ed.* **2021**, *60*, 3999-4003.
[36] P. Cheng, Q. Miao, J. Li, J. Huang, C. Xie, K. Pu, *J. Am. Chem. Soc.* **2019,** *141*, 10581-10584.
[37] J. Huang, J. Huang, P. Cheng, Y. Jiang, K. Pu, *Adv. Funct. Mater.* **2020**, *30*, 2003628.
[38] J. Cao, W. An, A. G. Reeves, A. R. Lippert, *Chem. Sci.* **2018**, *9*, 2552-2558.
[39] S. Ye, B. Yang, M. Wu, Z. Chen, J. Shen, D. Shabat, D. Yang, *CCS Chemistry* **2021**, *4*, 1871-1878.
[40] W. An, L. S. Ryan, A. G. Reeves, K. J. Bruemmer, L. Mouhaffel, J. L. Gerberich, A. Winters, R. P. Mason, A. R. Lippert, *Angew. Chem. Int. Ed.* **2019**, *58*, 1361-1365.
[41] N. Hananya, O. Green, R. Blau, R. Satchi-Fainaro, D. Shabat, *Angew. Chem. Int. Ed.* **2017**, *56*, 11793-11796.
[42] S. Ye, N. Hananya, O. Green, H. Chen, A. Q. Zhao, J. Shen, D. Shabat, D. Yang, *Angew. Chem. Int. Ed.* **2020**, *59*, 14326-14330.
[43] M. Yang, J. Zhang, D. Shabat, J. Fan, X. Peng, *ACS Sens.* **2020**, *5*, 3158-3164.
[44] K. J. Bruemmer, O. Green, T. A. Su, D. Shabat, C. J. Chang, *Angew. Chem. Int. Ed.* **2018**, *57*, 7508-7512.
[45] J. Cao, R. Lopez, J. M. Thacker, J. Y. Moon, C. Jiang, S. N. S. Morris, J. H. Bauer, P. Tao, R. P. Mason, A. R. Lippert, *Chem. Sci.* **2015**, *6*, 1979-1985.
[46] S. A. Almatroodi, C. F. McDonald, I. A. Darby, D. S. Pouniotis, *Cancer Microenviron.* **2016**, *9*, 1-11.
[47] A. Pompella, V. De Tata, A. Paolicchi, F. Zunino, *Biochem. Pharmacol.* **2006**, *71*, 231-238.
[48] a) H. Yan, Y. Wang, F. Huo, C. Yin, *J. Am. Chem. Soc.* **2023**, *145*, 3229-3237; b) K. Ma, Y. Yue, L. Zhao, J. Chao, C. Yin, *Chem. Commun*. **2021**, *57*, 10015-10018; c) P. Cheng, S. He, C. Zhang, J. Liu, K. Pu, *Angew. Chem. Int. Ed.* **2023**, *62*, e202301625; d) P. Cheng, R. Wang, S. He, P. Yan, H. Huang, J. Chen, J. Shen, K. Pu, *Angew. Chem. Int. Ed.* **2023**, *62*, e202306539; e) X. Wang, S. He, P. Cheng, K. Pu, *Adv. Mater.* **2023**, *35*, 2206510.
[49] S. Li, Q. Deng, Y. Zhang, X. Li, G. Wen, X. Cui, Y. Wan, Y. Huang, J. Chen, Z. Liu, L. Wang, C.-S. Lee, *Adv. Mater.* **2020**, *32*, 2001146.
[50] K. A. Ryu, L. Stutts, J. K. Tom, R. J. Mancini, A. P. Esser-Kahn, *J. Am. Chem. Soc.* **2014**, *136*, 10823-10825.
[51] C. Xu, J. Huang, Y. Jiang, S. He, C. Zhang, K. Pu, *Nat. Biomed. Eng.* **2023**, *7*, 298-312.

Entry for the Table of Contents

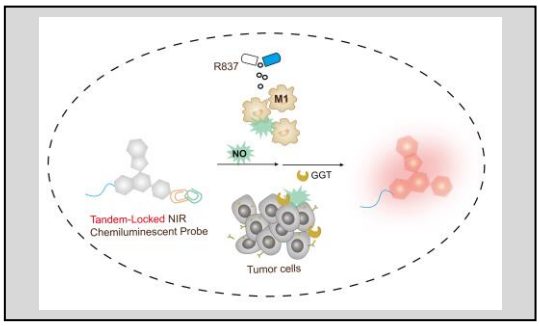

A hydrophilic tandem-locked probe based on a highly efficient chemiluminophore is developed to only activate chemiluminescent signal in the presence of both tumour and M1 macrophage biomarkers, enabling monitoring tumor-associated macrophage polarization.